

Photon emission in Pb+Pb collisions at SpS and LHC

D.Yu. Peressounko and Yu.E. Pokrovsky

RRC "Kurchatov Institute" 123182, Moscow, Kurchatov sq., 1.

e-mail: peres@pretty.mbslab.kiae.ru

Yield of direct photons in Pb+Pb collisions at SpS and LHC energy is evaluated with emphasis on estimate of possible uncertainty. Possibility of experimental observation of direct photons at LHC is discussed. Predictions of several models at SpS energy are compared with experimental data.

Photon emission is one of the most actively used observables both in present and developed heavy ion experiments. The reason is that photons, in contrast to hadronic probes, have extremely large free path length in the hot matter and escape from it without rescattering. This makes them a unique probe of the initial stage of collision, and the inner part of the created hot matter. In particular, direct photons are considered as one of the most promising signatures of quark-gluon plasma.

As well known, photons, emitted in the heavy ion collision, can be divided onto direct and decay ones. The direct photons are emitted as a result of rescatterings of charged particles in the hot matter. The decay photons are the photons, originated due to decays of final hadrons, mainly π^0 and η mesons. In addition to this, one can subdivide direct photons on prompt and thermal. Prompt photons are emitted in the very beginning of the collision in scatterings of charged constituents of target and projectile. They have approximately the same energy distribution as emitting particles – power one – and thus contribute mainly into the hard part of the spectrum. Thermal photons are emitted on the later stages of collision, when local thermodynamic equilibrium is almost reached. They have approximately exponential spectrum. Decay photons can be subdivided on photons, originated from decay of hadrons, emitted from QGP surface [1] and from hadronic gas, and therefore bring out information about two different phases of the hadron matter.

Despite a large number of papers devoted to photon emission in heavy ion collisions [2]- [29], it is not quite clear, how predictions of various models differ from each other, how strong is sensitivity of these predictions to the variations of model parameters, approximations, and assumptions of the models, and how reasonable are attempts to find photon signatures of QGP. These points are not discussed in the literature detailed enough to estimate simultaneously all important contributions to photon spectra in wide range of photon momentum. In this paper we made an attempt to compare predictions of various models in the common basis and estimate sensitivity of the predictions to the variations of the model parameters. Thus, basing on SpS data, we estimate possible uncertainties of predictions of direct and decay photon yield in Pb+Pb collisions at LHC. Having in mind present and developing experiments we restrict ourselves by *Pb* nuclei.

The plan of this paper is following. In the first part we consider yield of prompt photons and estimate uncertainty in their evaluations. In the second part we consider evaluation of emission rates of thermal photons from QGP and hadronic gas with and without chemical equilibrium. Having emission rates we evaluate yield of thermal photons accounting dynamics of the system within various hydrodynamic models and explore sensitivity to the model approximations. Then we compare predictions of cascade and hydrodynamic models at SpS energies. In the third part we consider decay photons and evaluate ratio Direct/Decay photons for various hydrodynamic and cascade models. Our results are summarized in the conclusion.

I. PROMPT PHOTONS.

Prompt photons are emitted in first interactions of charged constituents of target and projectile. Prompt photons reflect dynamics of the very beginning of collision, and can be used to study structure functions of colliding nuclei. To evaluate yield of prompt photons one should convolute momentum distributions of incident partons (structure functions of colliding nuclei) F with cross sections of elementary collisions $qg \rightarrow \gamma q$, $q\bar{q} \rightarrow \gamma g$, bremsstrahlung etc.

$$E_\gamma \frac{d\sigma}{d^3p_\gamma} = \sum_{a,b} \int \frac{dx_a dx_b}{x_a x_b} F(a, A; x_a) F(b, B; x_b) E_\gamma \frac{d\sigma_{ab \rightarrow c\gamma}}{d^3p_\gamma} \quad (1)$$

Due to the comparatively high momentum transfer, these cross-sections can be evaluated within perturbative QCD with reasonable accuracy. The main uncertainty in the prompt photon yield comes from structure functions: emission

of photon even with as high energy as $E_\gamma \sim 5 \text{ GeV}$ in Pb+Pb collision at $\sqrt{s} = 6300 A \cdot \text{GeV}$ is determined by structure functions in the low x region ($x \sim E_\gamma/\sqrt{s} \sim 0.001$), where they are not known well yet. In addition, one should take into account modifications of structure functions in nuclei, what further increase uncertainty in the yield of prompt photons.

This uncertainty is demonstrated on the fig. 1, where several evaluations with different structure functions are shown. Dotted line corresponds to the predictions of Alam et al. [7]. They used Duke and Owens, set I [30] parametrization of structure functions without accounting any modifications in nuclei. However, since this paper a new data on the low x behavior of structure functions was obtained, and in the paper [12], the yield of direct photons was evaluated with new parametrization (Gluck, Reya and Vogt [31]) of structure functions. This prediction is shown by solid line. As one can see, various parametrizations results in difference more then order of magnitude. In addition to this, structure functions in nuclei significantly differ from ones of single nucleon: depending on the value of x one finds shadowing, antishadowing, EMC effect, Fermi motion etc. As far as we are interesting in low x region, the shadowing is the most important for us. In the paper [12] Gluck-Reya-Vogt structure functions was modified to include this effect. This result is shown by dashed line.

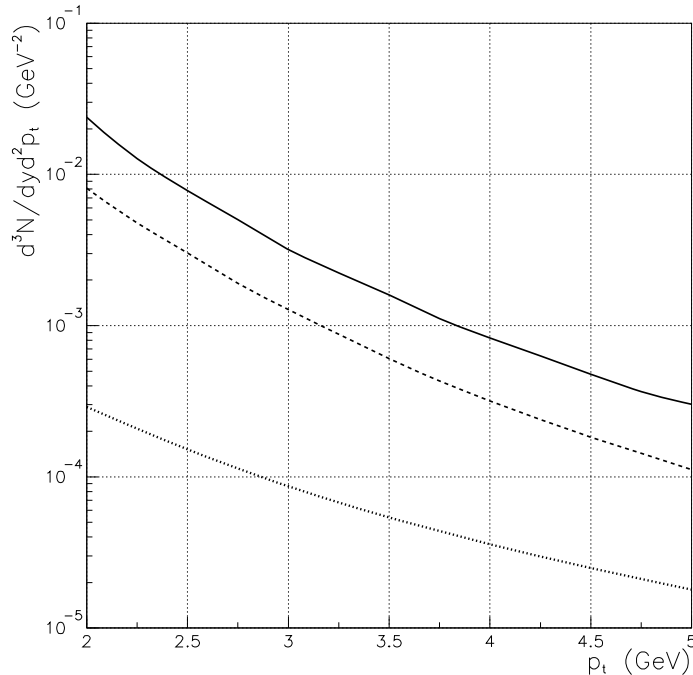


FIG. 1. Yield of prompt photons in $Pb + Pb$ collision at LHC energy, evaluated in [7,12] with structure functions of Duke and Owens, set I – dotted line, with Gluck, Reya and Vogt parametrization of structure functions without accounting of shadowing (solid line) and with shadowing (dashed line).

So that, using of different parametrizations of structure functions results in difference in the yield of prompt photons up to order of magnitude, while taking into account modifications of structure functions in nuclei varies it approximately in three times. On this background one can neglect uncertainties arising from higher order QCD corrections, which (estimated, e.g., from pp data) do not exceed a factor 2.

II. THERMAL PHOTONS

Evaluating yield of thermal photons, one assumes, that they are emitted from a medium at local thermal equilibrium. So that one can average individual collisions, producing photons, over time and volume and evaluate average number of photons, emitted from unit volume per unit time – emission rate R . In the case of perfect thermal equilibrium emission, the rate depends only on the temperature of the medium, however, in the absence of the chemical equilibrium it depends also on fugacities of quarks and gluons in QGP and hadrons in hadronic gas. When emission rates from QGP and hadronic gas are evaluated, one integrates these rates over space-time volume, occupied by the system, and finds total yield of thermal photons.

A. Emission rate from Quark-Gluon Plasma

Thermal photons are emitted from QGP due to reactions: $gq \rightarrow \gamma q$ (Compton scattering), $q\bar{q} \rightarrow g\gamma$ (annihilation), $qq \rightarrow \gamma qq$ (bremsstrahlung) and other processes with higher order in $\alpha = 1/137$ and $\alpha_s \sim 0.4$ – the strong coupling constant. To begin with, let us consider the simplest two-particle reactions: Compton scattering and annihilation. In this case, emission rate is described by the following formula, practically the same, as (1), but with thermal distributions instead of structure functions, Pauli blocking and Bose enhancement for final particles:

$$E \frac{dR}{d^4x d^3p} = \sum \int \prod_{i=1}^3 \frac{d^3p_i}{2E_i(2\pi)^3} f_1(p_1) f_2(p_2) [1 \pm f_3(p_3)] \frac{1}{2(2\pi)^3} |M|^2 (2\pi)^4 \delta^4(p_1 + p_2 - p_3 - p), \quad (2)$$

where sum is taken over all possible (two-particle) reactions, $f(p)$ – thermal distribution functions, $|M|^2$ – squared matrix element of the corresponding reaction.

Using $|M|$ evaluated at lowest order both in α and α_s , and taking thermal distributions, one obtains expression for emission rate [3]:

$$E \frac{dN}{d^4x d^3p} = \sum_{u,d,\dots} e_q^2 \frac{\alpha \alpha_s}{2\pi^2} T^2 e^{-E/T} \left[\ln \frac{ET}{m^2} + const \right]. \quad (3)$$

This expression diverges for massless quarks $m \rightarrow 0$. This is reflection of the well known Coulomb divergency. To screen it one has to take into account medium effects. This was done in [13] using Braaten-Pisarski technique of hard thermal loops. As a result of this calculations current mass of quarks m was changed to screening mass $\bar{m}^2 = g^2 T^2 / 2.912$ ($\alpha_s = g^2 / 4\pi$) what results in the rate:

$$E \frac{dN}{d^4x d^3p} = \sum_{u,d,\dots} e_q^2 \frac{\alpha \alpha_s}{2\pi^2} T^2 e^{-E/T} \ln \left(\frac{2.912E}{g^2 T} \right). \quad (4)$$

Emission rate, evaluated at $T = 0.2 \text{ GeV}$, $\alpha_s = 0.4$ for plasma, consisting of two flavor quarks and gluons is shown on the fig. 2 by dashed line. To perform these calculations analytically, Boltzmann distributions was used instead of Fermi and Bose ones. In case of Bose and Fermi distributions one can perform evaluations numerically. It was shown in [13] that one can fit this result by function (4) with argument of \ln changed to $2.912E/g^2T + 1$. Corresponding curve is shown on the fig. 2 by solid line, marked by rectangles.

Let us now return to the more complicated processes – bremsstrahlung and annihilation with scattering on third quark. These processes arises in the next order of α_s , compared to Compton scattering and annihilation. It is well known, that in vacuum the bremsstrahlung contribute mainly into the soft part of spectrum. So one usually neglects its contribution into thermal photon emission. However, recently it was shown [14], that in thermal QCD these processes appear to be important and even dominate over compton scattering and annihilation even in hard part of spectrum. In this paper in framework of hard thermal loop technique an expression was obtained for emission rate of hard ($E_\gamma > T$) photons due to bremsstrahlung:

$$E \frac{dN}{d^4x d^3p} = \sum_{u,d,\dots} e_q^2 \frac{8}{\pi^5} \alpha \alpha_s T^2 e^{-E/T} (J_T - J_L) \ln 2 \quad (5)$$

and due to annihilation with scattering on third quark:

$$E \frac{dN}{d^4x d^3p} = \sum_{u,d,\dots} e_q^2 \frac{8}{3\pi^5} \alpha \alpha_s E T e^{-E/T} (J_T - J_L), \quad (6)$$

where, for two quark flavors constants $J_T \approx 4.45$ and $J_L \approx -4.26$. It is interesting, that this contributions have the same order in α_s as two-particle reaction. This takes place because of the presence of collinear divergency in matrix element of reaction, which is screened by quark mass. This results in enhancement factor $\sim 1/m_q^2 \sim 1/g^2$. Sum of these two contributions into thermal photon emission rate is shown on fig. 2 by thick solid line. As one can see, taking into account of these processes increases significantly (up to order of magnitude) emission rate.

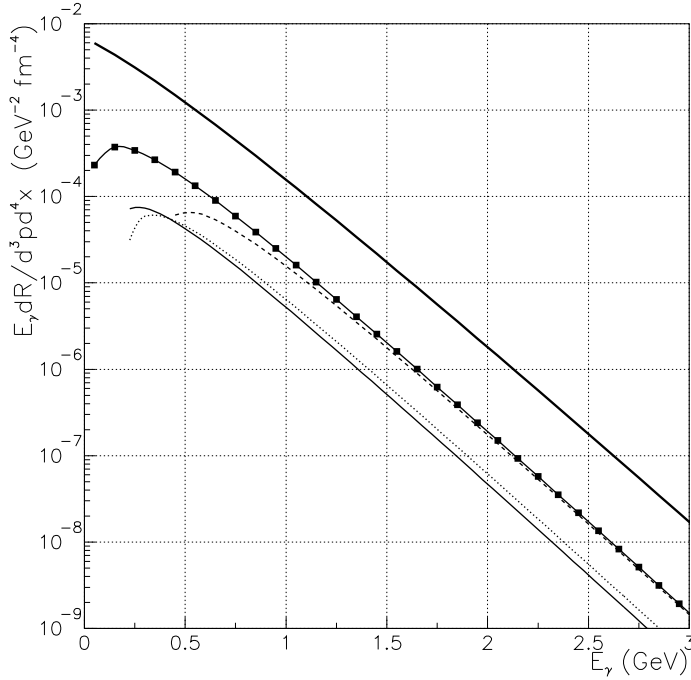


FIG. 2. Emission rates of thermal photons from QGP at $T = 200 \text{ MeV}$. Thick solid line – emission rate with accounting of bremsstrahlung and annihilation with rescattering on third particle. Solid line with rectangles and dashed line correspond to emission rates from Compton scattering and annihilation with Bose-Fermi and Boltzmann thermal distributions correspondingly. Dotted line and thin solid line – chemically nonequilibrated QGP with $\lambda_q = 0.5$, $\lambda_g = 1$ and $\lambda_q = 0.5$, $\lambda_g = 0.5$ correspondingly, only Compton scattering and annihilation are taken into account.

If QGP is formed in the nucleus-nucleus collision, then the number of quarks and gluons in it may be much lower, than in the plasma at perfect chemical equilibrium. This can strongly affect on the emission rate [15–17]. The simplest way to account undersaturation of quarks in the QGP is just to put coefficient λ_q (fugacity of quarks) as a coefficient in the emission rate. More advanced possibility is in addition to this to evaluate screening masses, depending on quark and gluon fugacities. However, in the case of absence of chemical equilibrium one can not be sure that there will be perfect screening of the column divergency as in the equilibrated case. In the paper [16] it was shown, that even in the case of absence of chemical equilibrium divergencies cancels each other in the emission rate. In particular case of distributions of quarks and gluons:

$$f_g(p) = \begin{cases} \lambda_g n_B(|p_0|), & p_0 > 0, \\ -[1 + \lambda_g n_B(|p_0|)], & p_0 < 0 \end{cases} \quad f_q(p) = \begin{cases} \lambda_q n_F(|p_0|), & p_0 > 0, \\ 1 - \lambda_q n_F(|p_0|), & p_0 < 0 \end{cases} \quad (7)$$

it was shown, that screening mass is

$$\bar{m}^2 = \frac{g^2 T^2}{9} \left(\lambda_g + \frac{\lambda_q}{2} \right)$$

and emission rate is given by formula

$$E \frac{dN}{d^4 x d^3 p} = \sum_{u,d,\dots} e_q^2 \frac{\alpha \alpha_s}{2\pi^2} \lambda_q T^2 e^{-E/T} \left[\frac{2}{3} \left(\lambda_g + \frac{\lambda_q}{2} \right) \log \left(\frac{2ET}{\bar{m}_q^2} \right) + \frac{4}{\pi^2} C(E, T, \lambda_q, \lambda_g) \right], \quad (8)$$

where

$$C(E, T, \lambda_q, \lambda_g) = \lambda_q \left[-1 + \left(1 - \frac{\pi^2}{6} \right) \gamma + \left(1 - \frac{\pi^2}{12} \right) \ln \frac{E}{T} + \zeta_- \right] + \lambda_g \left[\frac{1}{2} + \left(1 - \frac{\pi^2}{3} \right) \gamma + \left(1 - \frac{\pi^2}{6} \right) \ln \frac{E}{T} - \zeta_+ \right] \\ + \lambda_q \lambda_g \left[\frac{1}{2} - \frac{\pi^2}{8} + \left(\frac{\pi^2}{4} - 2 \right) \left(\gamma + \ln \frac{E}{T} \right) + \frac{3}{2} \zeta'(2) + \frac{\pi^2}{12} \ln 2 + \zeta_+ - \zeta_- \right]$$

and $\gamma = 0.577\dots$ – Euler constant, $\zeta_+ = \sum_{n=2}^{\infty} \frac{1}{n^2} \ln(n-1) \approx 0.67$, $\zeta_- = \sum_{n=2}^{\infty} \frac{(-1)^n}{n^2} \ln(n-1) \approx -0.04$ and ζ' – derivative of Riemann ζ -function ($\zeta'(2) = -2.404$).

In the case $\lambda_q = 1$ and $\lambda_g = 1$ this formula coincides with (4). Emission rates, evaluated with this formula are shown on fig. 2 by dotted line ($\lambda_q = 0.5, \lambda_g = 1$) and solid line ($\lambda_q = 0.5, \lambda_g = 0.5$). As one can see, emission rate is very sensitive to the undersaturation of charged constituents, while undersaturations of gluons slightly vary emission rates.

There are three main sources of uncertainties of emission rate. First – contributions from higher order in α_s processes. As we have seen, taking into account bremsstrahlung and annihilation with scattering on third particle in addition to Compton scattering and annihilation result in increasing of emission rate up to order of magnitude. So one can not be sure that inclusion of processes of the next order in α_s does not result in similar changes of emission rate. Second – all considered evaluations are performed in the framework of Braaten - Pisarski Hard Thermal Loop technique, applicable for the case $g \ll 1$. To evaluate yield of thermal photons in the heavy ion collisions we have to extend these results for the case $\alpha_s \sim 0.4$ e.g. $g \sim 2$. Third – in our evaluations we consider region $E_\gamma \gg T$ – the right tail of the thermal distribution. It is well known, that thermal distribution on the tails forms much more slower, than in the region $E \sim T$, where 1-2 collisions are sufficient for establishing of thermal equilibrium. So, if temperature is rapidly changes with time, then long tail is not able to form, and it is the region, where this effect is important. In contrast to the first two sources, the last effect results in changing of the shape of the distribution and can even result in nonexponential distribution.

B. Emission rate from hadronic gas

Thermal photons can be emitted from hadronic gas as a result of reactions $\pi\pi \rightarrow \rho\gamma$, $\pi\rho \rightarrow \pi\gamma$, $\rho \rightarrow \pi\pi\gamma$, $\pi\pi \rightarrow \eta\gamma$ etc. In the paper [13] it was shown, that processes $\pi\rho \rightarrow \pi\gamma$ plays the dominant role in emission of photons with energy larger than $\sim 0.7 GeV$. In addition, it was shown, that photon emission of the hadronic matter is very similar to the photon emission of QGP (including only Compton scattering and annihilation) at the same temperature. So one can parametrize photon emission rate from hadronic gas in the form (4). Emission rate of hadronic gas, evaluated at $T = 180 MeV$ in accordance with this parametrization is shown on fig. 3 by solid line.

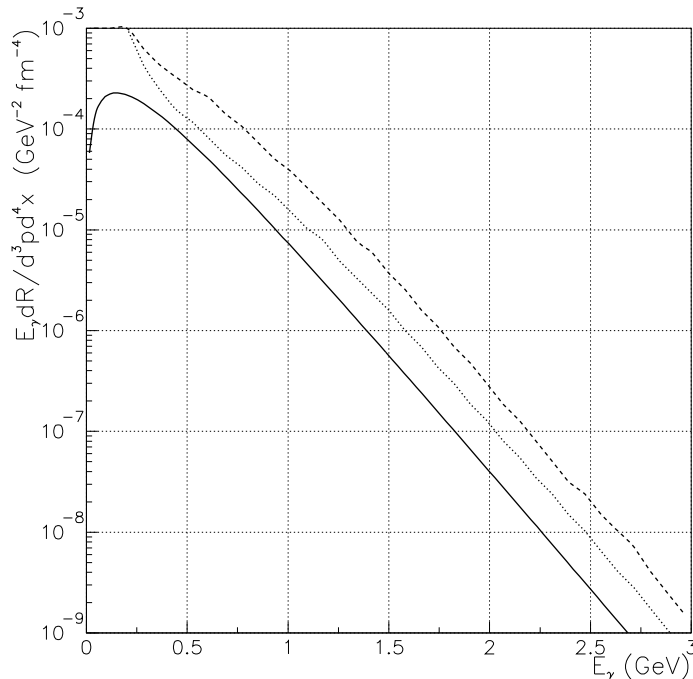


FIG. 3. Emission rates of thermal photons from hadronic gas at $T = 180 MeV$, evaluated with emission rate (4) (solid line), with accounting of a_1 resonance (9) (dotted line), and with accounting of in-medium effects (dashed line).

Later it was shown [18], that contribution of A_1 resonance into process $\pi\rho \rightarrow A_1 \rightarrow \pi\gamma$ is important: it increase emission rate approximately twice. There was proposed following parametrization of emission rate with accounting

of contribution of A_1 resonance:

$$E \frac{dR}{d^4x d^3p} = 2.4 T^{2.15} \exp(-1/(1.35 T E)^{0.77} - E/T) \quad (fm^{-4} GeV^{-2}) \quad (9)$$

Considered emission rates are evaluated with vacuum masses and widths of hadrons. However, these properties change in medium, so that evaluated emission rates should change too. In the paper [19] an attempt was made to evaluate photon emission rate with accounting of such effects. Effective Lagrangian approach was used to evaluate in-medium masses and widths. It was shown, that due to decreasing of vector meson masses yield of thermal photons increases. These predictions for hadronic gas at $T = 180 MeV$ are shown on the fig. 3 by dashed line.

From one hand, situations with emission rate from hadronic gas is almost so shaky as with emission rate from QGP – as far as there is no theory of strong couplings. From the other hand, one can normalize coupling constants and other hadronic properties to experiment as it was done in [18], what can not be done in the case of QGP. In addition to this, evaluated emission rates suppose chemical equilibrium. However, it may not be established due to various reasons: fashion of hadronization of QGP, fast cooling of hadronic gas, fly out of hadrons from QGP surface [1] and hadronic gas, etc. As it was shown e.g. in [13], main contribution to emission rate comes from pion-pion and pion-rho scatterings. So, the most important for us is oversaturation of pions and rho due to fast cooling. One can estimate this oversaturation as ratio $N(T_c)/N(T_f) \sim (T_c/T_f)^3$, where T_c and T_f – transition and freeze-out temperatures correspondingly. So one could expect, that emission rate increase in the same ratio. So we estimate uncertainty in emission rate from hadronic gas within factor ~ 3 due to in-medium effects and factor ~ 3 due to oversaturation of pions and rho in hadronic gas.

C. Yields of thermal photons

To evaluate yield of thermal photons in the nucleus-nucleus collision one should convolute emission rate with space-time evolution of the system:

$$E_\gamma \frac{dN}{d^3p} = \int E_\gamma \frac{dR}{d^3p}(T) dV dt \quad (10)$$

Below we consider several models of evolution of hot matter and evaluate yield of thermal photons in these models.

First of all, on the example of very simple 1+1 (1 space+ time) Bjorken hydrodynamic model [20] we show main phenomena: dependence on initial conditions, transition temperature etc., and then compare predictions of Bjorken model with 1+1 Landau hydrodynamics and more advanced model such as (2+1) Bjorken model.

In the 1+1 Bjorken hydrodynamic model of evolution of heavy ion collision it is assumed, that hot matter, created in the beginning of collision, expands only longitudinally (along collision axis) and longitudinal velocity depends on longitudinal coordinate in the following way:

$$u^\mu = \left(\frac{t}{\tau}, 0, 0, \frac{z}{\tau} \right), \quad \tau = \sqrt{t^2 - z^2}.$$

This parametrization of velocity result in flat rapidity distribution of fluid elements, and as a result – of final hadrons. So, this model is well applicable only in the midrapidity region. Below we restrict ourselves by midrapidity region $z = 0$, $\tau = t$, because this region is most interesting from point of view of observation of hot hadronic matter.

As a result of such expansion, the volume of the hot matter increase with time in the following way:

$$V = 2\pi R^2 t,$$

where R – radius of colliding nuclei. If one assumes now, that entropy is conserved during all the expansion, one can relate temperature and time:

$$S = s \cdot V = const \cdot \left(\frac{dN}{dy} \right), \quad s = 4 \frac{\pi^2}{90} g T^3$$

or

$$T^3 t = \frac{\pi}{\zeta(3) R^2 g} \frac{dN}{dy},$$

where T – temperature, t – time, g – degeneracy, dN/dy – multiplicity of final (massless) hadrons (bosons) and $\zeta(3) = 1.202$. In the simplest version of Bjorken hydrodynamics we have $g_{QGP} = 16 + \frac{7}{8}24$ for degeneracy of QGP and $g_{hadr} = 3$ for hadronic gas with dominating pions.

Now, choosing from some considerations e.g. from cascade model multiplicity dN/dy and initial time (initial temperature) – the time (temperature), at which we already can assume thermal equilibrium, we find initial conditions. Then, fixing transition temperature T_c and freeze-out temperature T_f , we completely define this model.

Having emission rate of photons (e.g. (4)) and description of evolution, one can evaluate the total number of thermal photons as function of model parameters:

$$N_\gamma \sim \left(\frac{dN}{dy}\right)^2 \left\{ \frac{1}{g_h^2 T_f^2} - \frac{2g_{QGP}^2 - g_h^2}{3g_{QGP}^2 g_h^2} \frac{1}{T_c^2} - \frac{1}{g_{QGP}^2} \frac{1}{T_{in}^2} \right\}. \quad (11)$$

As one can easily see, the total number of thermal photons slightly depends on the initial temperature, but strongly – on freeze-out one. This is due to emission of very soft photons during prolonged evolution in the case of lower T_f . However, we are interested in the hard part of the spectra, so that this quantity is not appropriate for our purposes. More informative would be p_t distribution of thermal photons.

Let us now fix basic set of parameters of the model:

$$dN/dy = 12000, \quad T_{in} = 1 \text{ GeV}, \quad T_c = 160 \text{ MeV}, \quad T_f = 100 \text{ MeV}, \quad (12)$$

and look, how p_t distribution of direct photons depends on variation of model parameters.

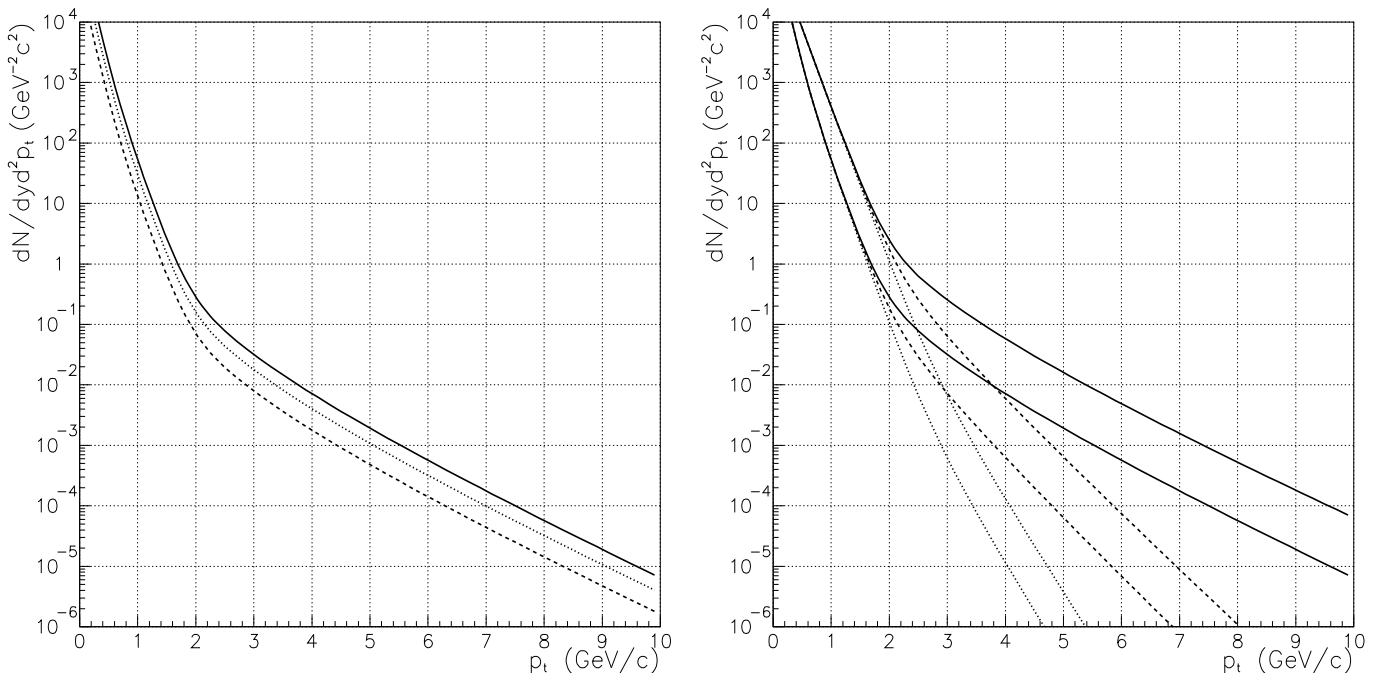


FIG. 4. Yield of thermal photons in $Pb + Pb$ collision at LHC energy within 1+1 Bjorken hydrodynamics. Left plot: yield evaluated using emission rate (4) both for QGP and hadronic phase and parameters (12) for $dN/dy = 12000$ (solid line), $dN/dy = 9000$ (dotted line) and $dN/dy = 6000$ (dashed line). Right plot: Yield, evaluated with parameters (12) and initial temperatures: $T_{in} = 1 \text{ GeV}$ (solid lines), $T_{in} = 500 \text{ MeV}$ (dashed lines) and $T_{in} = 300 \text{ MeV}$ (dotted lines). Upper three curves evaluated using emission rates (5),(6) for QGP phase, and (9) for hadronic phase, bottom three curves – using emission rate (4) both for QGP and hadronic phase.

To begin with, let us vary multiplicity – see fig. 4. With fixed initial temperature variation of dN/dy means variation of initial time, and thus all times of the evolution: all times change in the same scale. As one can expect from (11), the number of photons varies as squared multiplicity, while the shape of distribution does not changes. However, this effect holds only for 1+1 Bjorken hydrodynamics. In more realistic models the dependence of dN^γ/dy on the total multiplicity is weaker. For example in the 2+1 Bjorken hydrodynamics $N^\gamma \sim (dN/dy)^{1.2}$ [21]. This can be understood

in the following way. The number of thermal photons is proportional to the number of charged particles times the number of collisions, suffered by each particle:

$$N_\gamma \sim N_{ch}\nu.$$

For the case of long lived system each particle can collide to all other particles, so $\nu \sim N_{ch}$. However, if system expands, or has final dimensions comparable or even less than free path length, then the number of collisions

$$\nu \sim \frac{D}{\lambda}$$

where D - dimensions of the system. In the case of 1+1 Bjorken hydrodynamics increasing of dN/dy result in increasing of longitudinal dimensions of the system at fixed transverse sizes, so $D \sim dN/dy$

$$N_\gamma \sim (dN/dy)^2.$$

If we allow transverse expansion, then $D \sim (dN/dy)^{1/3}$ and

$$N_\gamma \sim (dN/dy)^{4/3},$$

result very close to obtained in 2+1 Bjorken hydrodynamics.

As a next step we vary initial temperature – see fig. 4, right plot. With fixed dN^π/dy this means that we cut off initial stages of evolution: in the case $T_{in} = 500 MeV$ we skip time $\tau = 0.15 \rightarrow 1 fm/c$ with respect to the case $T_{in} = 1 GeV$ and in the case $T_{in} = 300 MeV$ – $\tau = 0.15 \rightarrow 4.6 fm/c$. So, from fig. 4 one can find what part of spectrum is formed at each stage of collision. We obtain very natural result: the harder part of spectrum is populated due to emission from the hottest stage of collision. In addition, on this figure we compare yields of thermal photons, evaluated using simplest emission rate (4) (three lowest curves) and emission rates, accounting second order QCD corrections (5,6) and a_1 contribution (9) (three upper curves). In the latter case yield of thermal photons is approximately order of magnitude larger.

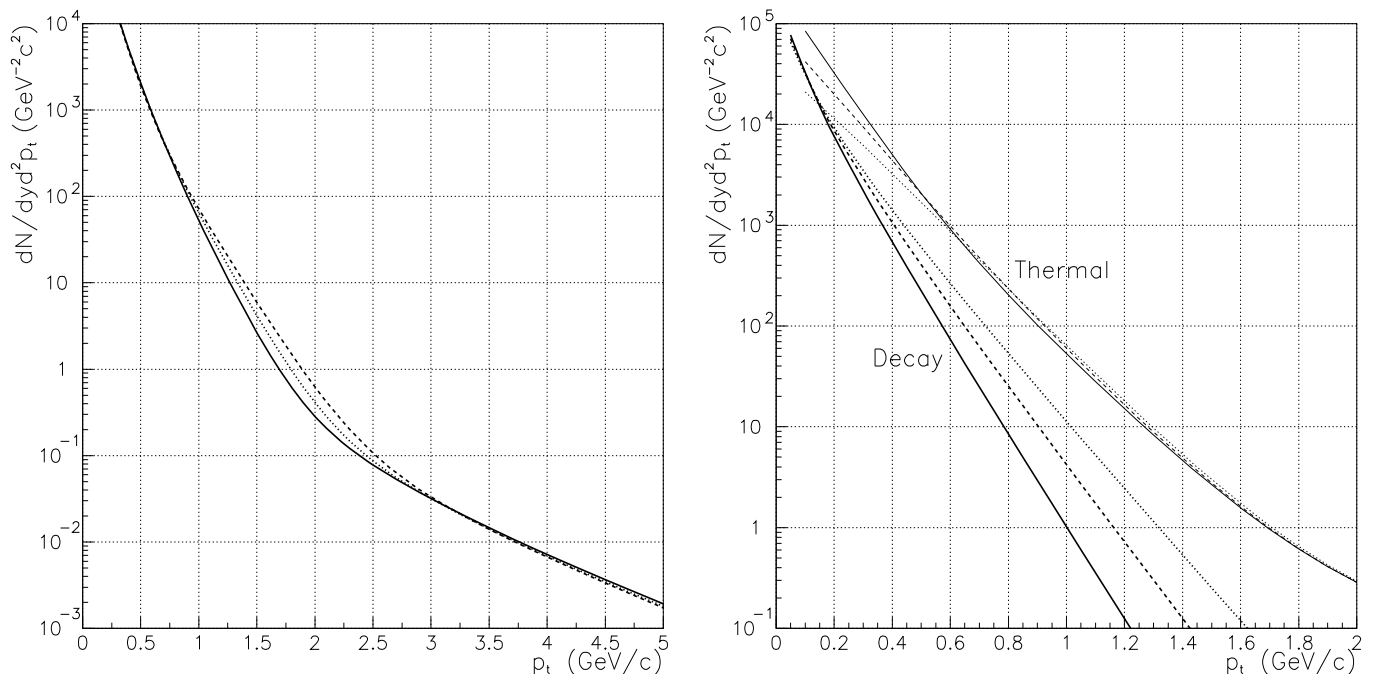


FIG. 5. Left plot: The same as fig. 4, but with different transition temperatures $T_c = 200 MeV$ (dashed line), $T_c = 180 MeV$ (dotted line) and $T_c = 160 MeV$ (solid line). Right plot: thermal and decay photons evaluated within 1+1 Bjorken hydrodynamics with different freeze-out temperatures: $T_f = 100 MeV$ (solid line), $T_{freeze} = 120 MeV$ (dashed line) and $T_c = 140 MeV$ (dotted line). In all cases thermal photons are evaluated with emission rate (4).

Next step is variation of the transition temperature T_c – see fig. 5, left plot. As we see below, mixed phase lives much more longer, than QGP phase, and thus a lot of thermal photons are emitted with $T = T_c$, increasing yield of medium energy direct photons with increasing of T_c . Lifetime of mixed phase is determined by ratio of degeneracies of QGP phase and hadronic phase. The simplest Equation of State (EOS) of hadronic gas corresponds to ideal gas of massless pions, so that this ratio is $37/3 \approx 12$ and mixed phase lives a very long time. If one considers hadronic gas, consisting from all known hadrons with masses below $2 GeV$, then this ratio becomes $37/12 \approx 3$ and time of life of mixed phase is significantly reduced, reducing yield of medium energy photons.

And finally we vary freeze-out temperature T_f . Its variation affects both p_t distributions of thermal photons and p_t distributions of final hadrons, and thus decay photons – so that we show both decay and direct photons on the fig. 5, right plot. From one hand, decreasing of T_f result in increasing of time of life of hadronic gas and thus yield of soft thermal photons, from the other hand it result in decreasing of the temperature of final hadrons, so that ratio *thermal/decay* increase.

Comparing figs. 4-5, one can conclude, that within 1+1 Bjorken hydrodynamic model hard part of spectrum of thermal photons $p_t > 2 GeV/c$ is governed by emission from the hottest region (QGP), variation of transition temperature vary p_t distribution at $1 < p_t < 2.5 GeV/c$, while the softest part of the spectrum $p_t < 0.5 GeV/c$ depends on the freeze-out temperature.

It is remarkable (see fig. 5, right plot), that within 1+1 Bjorken hydrodynamics direct photons dominate over decay ones practically at all energies. We obtain this unphysical result because we neglect transverse expansion. In the case of thermal photons absence of transverse expansion result in extremely large times of evolution: e.g. for our set of parameters (12) we find

$$\tau_0 = 0.15 fm/c, \quad \tau_{qgp} = 12 fm/c, \quad \tau_{mixed} = 137 fm/c, \quad \tau_f = 560 fm/c, \quad (13)$$

where τ_0 – time of thermalization, τ_{qgp} – time of disappearing of QGP, τ_{mixed} – time of disappearing of mixed phase, τ_f – time of freeze-out. So that, emission of photons from the mixed phase and especially from the hadronic phase is strongly overestimated in comparison with the models with transverse expansion.

In the case of decay photons, absence of transverse expansion result in lower effective temperature, and smaller contribution with respect to thermal photons.

However, this does not mean, that 1+1 Bjorken model is useless: as we see below, it makes reasonable predictions for hard part $p_t > 2 GeV/c$ of the spectrum of thermal photons, emitted on the stage, where transverse expansion is not very important.

Bjorken model of evolution is essentially nonhydrodynamic, i.e. it is not solution of the hydrodynamic equations. So, it is interesting to compare its predictions with really hydrodynamic model e.g. 1+1 Landau hydrodynamics [22]. Within this model it is assumed, that just after penetration of colliding nuclei through each other a thermalized matter is created, having form of Lorentz compressed disk. The part of the total energy, deposited in this disk is model parameter – coefficient of inelasticity K . Being formed, disk expands along beam axis in accordance with one dimensional hydrodynamic equations. Initially disk has size along beam axis:

$$\Delta = \frac{4m_p R}{3K\sqrt{s}} \frac{c_s^2}{1 + c_s^2}, \quad (14)$$

where m_p is the proton mass, K – coefficient of inelasticity $K \sim 0.5$, R – radius of nucleus and c_s^2 – speed of sound in the created matter. For $Pb + Pb$ collision ($R = 6.5 fm$) at LHC energy ($\sqrt{s} = 6300 A \cdot GeV$) one finds ($K = 0.5, c_s^2 = 1/3$):

$$\Delta \approx 0.0025 fm.$$

Initial temperature can be evaluated from the condition

$$2\pi R^2 \Delta \cdot \varepsilon = K\sqrt{s} \cdot A,$$

where ε -energy density. Assuming QGP consisting of two quark flavors and gluons, one finds for $Pb + Pb$ collisions at LHC energy:

$$T_{in} = 5.1 GeV.$$

Result of evaluation of the yield of thermal photons from QGP phase only ($T_c = 220 MeV$) within Landau model taken from [22] is presented on the fig. 6 by solid line. Dashed line corresponds to the evaluation within 1+1 Bjorken

model with the same initial conditions: $T_{in} = 5.1 \text{ GeV}$, $T_c = 220 \text{ MeV}$ and $\tau_{in} = 0.0025 \text{ fm}/c$. This conditions correspond to multiplicity $dN^\pi/dy = 5300$. As one can see, lines goes rather close to each other, though there is some difference due to different rapidity distributions and, as a consequence, different dependence $T(\tau)$. Scaling expansion result in faster cooling in the beginning and slower – on the later stages. Nevertheless, this result demonstrate, that use of scaling longitudinal expansion instead of hydrodynamic one is not critical for our purposes.

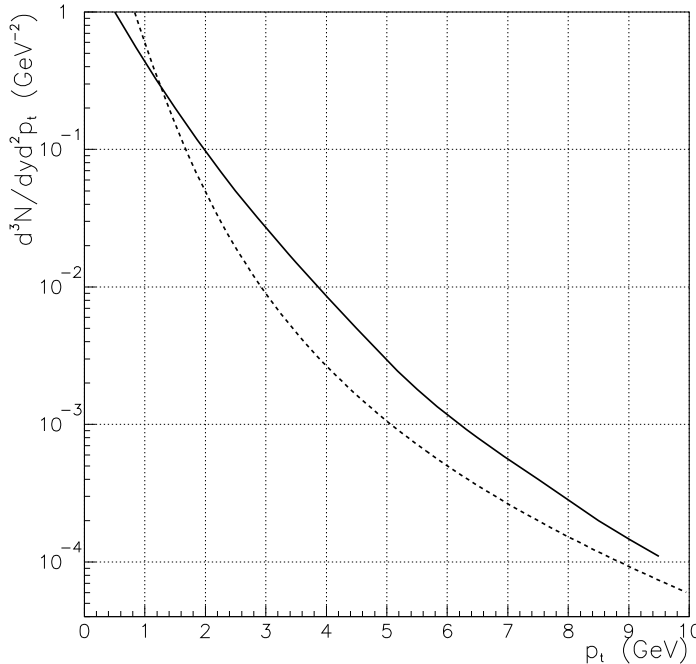


FIG. 6. Yield of thermal photons, emitted from QGP phase in $Pb + Pb$ collision at LHC energy, evaluated within Landau hydrodynamic model (solid line), and 1+1 Bjorken hydrodynamics with $T_0 = 5.1 \text{ GeV}$, $T_c = 220 \text{ MeV}$ and $\tau_{in} = 0.0025 \text{ fm}/c$ (dashed line).

Taking into account transverse expansion alters significantly all evolution of the system, and thus spectra of the thermal photons. To include transverse expansion we consider 2+1 Bjorken hydrodynamics. This means, that we assume Bjorken scaling expansion along beam axis, while for expansion in transverse direction we solve hydrodynamic equations. So, we parametrize 4-velocity in the form:

$$u^\mu = \gamma \left(\frac{t}{\tau}, \vec{v}_r, \frac{z}{\tau} \right) \quad \tau = \sqrt{t^2 - z^2}, \quad \gamma = (1 - v^2)^{-\frac{1}{2}},$$

and solve hydrodynamic equations

$$\partial_\mu T^{\mu\nu} = 0, \quad T^{\mu\nu}(x) = (\varepsilon(x) + p(x)) \cdot u^\mu u^\nu - g^{\mu\nu} \cdot p(x), \quad (15)$$

where $T^{\mu\nu}$ – energy-momentum tensor of ideal fluid, $\varepsilon(x)$ and $p(x)$ – local energy density and pressure correspondingly, u^μ – 4-velocity and $g^{\mu\nu}$ metric tensor ($g = \text{diag}(1, -1, -1, -1)$). In the case of cylindrically symmetrical transverse expansion and longitudinal scaling expansion one can rewrite (15) in the form

$$\begin{aligned} \partial_\tau (\gamma^2 w) + \partial_r (\gamma^2 v w) + \gamma^2 w \tau^{-1} + \gamma^2 v w r^{-1} - \partial_\tau p &= 0 \\ \partial_\tau (\gamma^2 v w) + \partial_r (\gamma^2 v^2 w) + \gamma^2 v w \tau^{-1} + \gamma^2 v^2 w r^{-1} + \partial_r p &= 0, \end{aligned} \quad (16)$$

where $w = \varepsilon + p$ – enthalpy density. We solve this equations numerically.

As in the one dimensional case we fix basic set of parameters

$$dN/dy = 12000, \quad T_{in} = 1 \text{ GeV}, \quad T_c = 160 \text{ MeV}, \quad T_f = 140 \text{ MeV}. \quad (17)$$

In contrast to the 1+1 dimensional case, where all time scales are given by initial time (at fixed initial temperature), in the 2+1 dimensional case we have two completely different time scales: one of longitudinal expansion – the same

as in 1+1 dimensional case and one of transverse expansion, determined by velocity of sound and dimensions of the system. So that, picture of expansion become much more complicated. Typical evolution of hot matter in 2+1 dimensional case is shown on the fig. 7 – this is result of evaluations with parameters, listed in (17) (left plot) and $dN/dy = 6000$, $T_{in} = 1 GeV$, $T_c = 160 MeV$, $T_f = 140 MeV$ (right plot). Initially system has zero transverse collective velocity, than due to acceleration in the QGP phase matter possesses velocity more then $0.7 \cdot c$. In the mixed phase pressure gradient is absent and velocities are constant (velocity levels are straight), and after the end of the mixed phase during hadronic gas expansion matter begins to accelerate further (slopes of velocity levels changed).

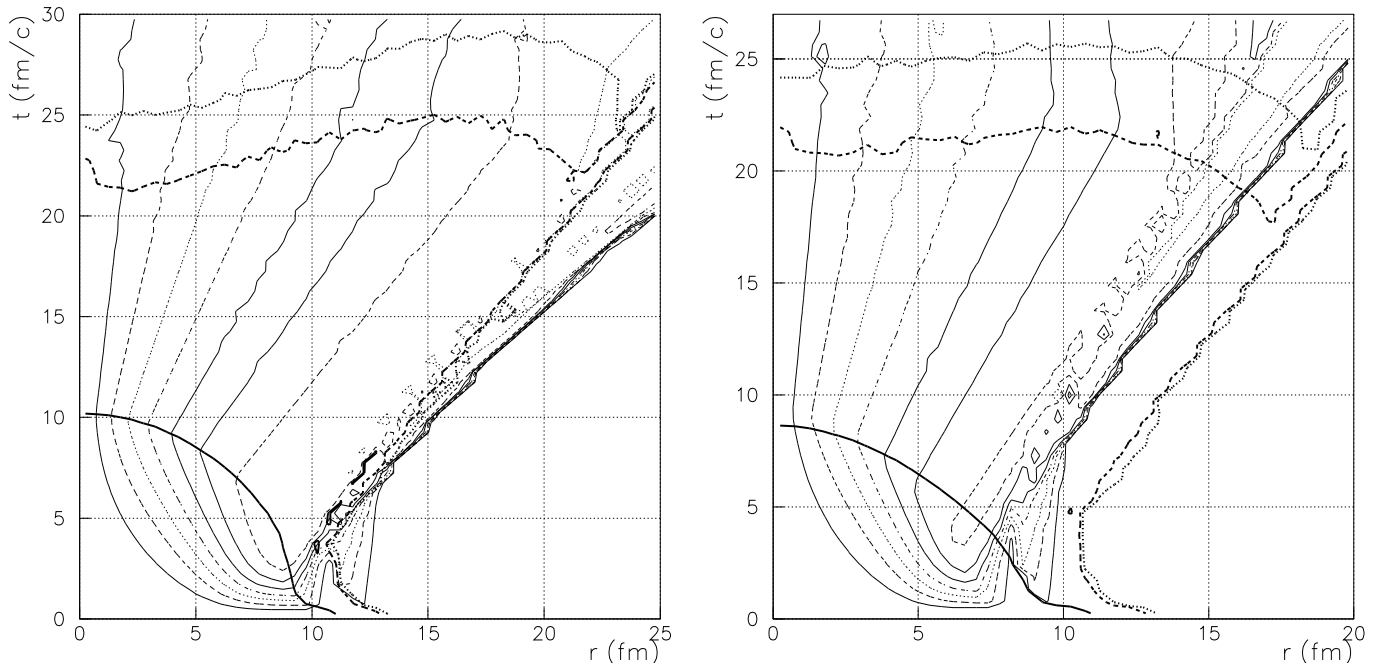


FIG. 7. Evolution of the hot matter, calculated at LHC energy for $dN/dy = 12000$ left plot, and $dN/dy = 6000$ right plot. Constant velocity levels (thin lines) are drawn at 0.1, 0.2, ... and constant energy density levels, are drawn at the boundary of QGP phase (thick solid line), at the boundary of mixed phase (thick dashed line) and freeze-out surface (thick dotted line).

In contrast to one dimensional case, times of life of mixed and hadronic phases is much smaller:

$$\tau_0 = 0.11 fm/c, \quad \tau_{qgp} = 10 fm/c, \quad \tau_{mixed} = 25 fm/c, \quad \tau_f = 30 fm/c. \quad (18)$$

in the case of $dN/dy = 12000$, and

$$\tau_0 = 0.06 fm/c, \quad \tau_{qgp} = 8 fm/c, \quad \tau_{mixed} = 22 fm/c, \quad \tau_f = 25 fm/c. \quad (19)$$

in the case of $dN/dy = 6000$.

In the case of larger multiplicity initial time is twice larger, so that in the beginning stage system cools twice slower, and more energy is spent to the developing of the radial velocity. Thus we find higher transverse collective velocity in the case of higher multiplicity. However, later stages ($t > 5 fm/c$) are governed mainly by radial expansion, so that life times of QGP, mixed phase and hadronic gas are very similar on both cases.

There are two important consequences of introduction of transverse expansion. First, – times of life are changed: time of life of QGP is changed slightly, but time of life of mixed phase and hadronic gas are reduced more then order of magnitude compared to 1+1 dimensional case. Second, – hot matter poses significant radial velocity, which affect spectrum of thermal photons and even in the more degree – spectrum of decay photons.

As a result of producing of the large radial velocity the thermal photons, emitted from hadronic gas contribute into the hard part of the spectrum of direct photons – see fig. 8. On these figures contributions of different times into the total yield of thermal photons are shown. Similar to one dimensional case, photons emitted at first several fm/c populate hard part of spectrum. However, due to high collective velocities contributions of later (cooler) stages into hard region are comparable with emission from the hottest stage. This effect is better pronounced in the case of higher multiplicity ($dN/dy = 12000$), where collective velocity can reach $v_r \sim 0.9$ and effective temperature

$$T_{eff} \sim T_f \sqrt{\frac{1+v_r}{1-v_r}} \sim 0.14 \text{ GeV} \cdot 4.4 \sim 0.6 \text{ GeV} \quad (20)$$

is comparable even with initial temperature.

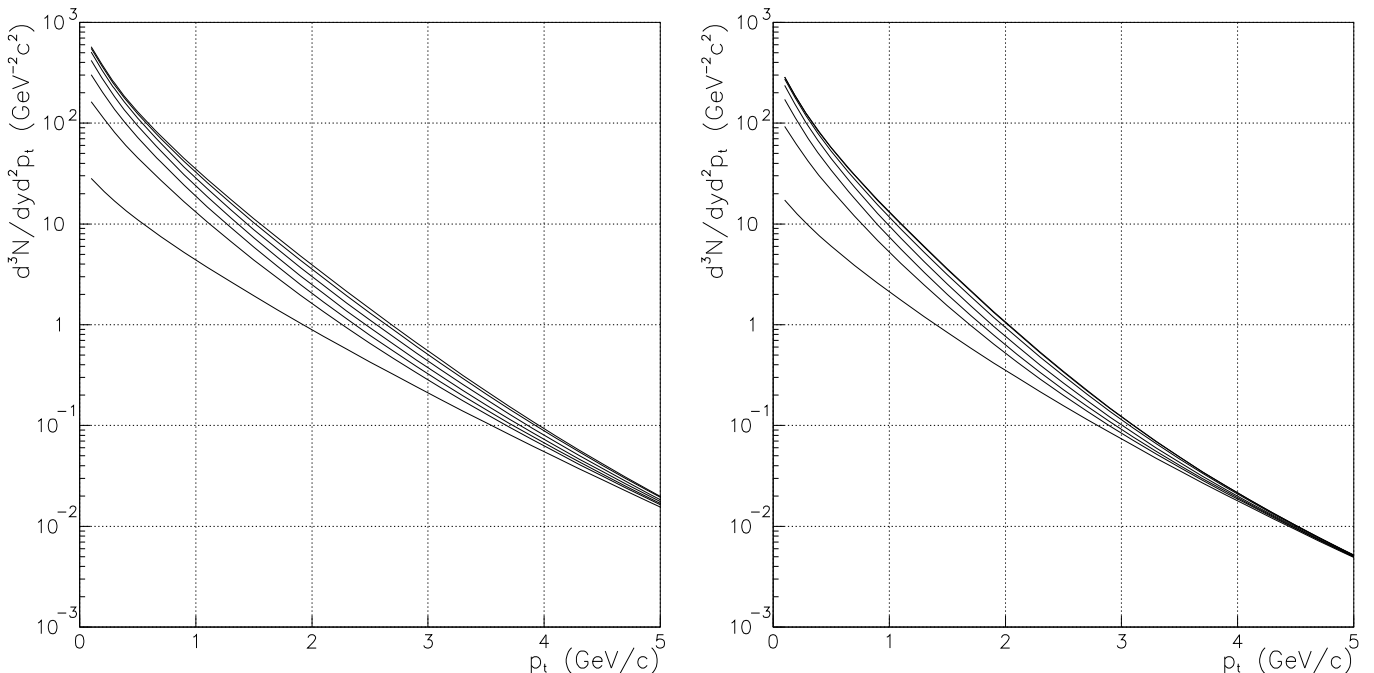


FIG. 8. Contributions of different times (from down to up 0-1, 0-5, 0-10, 0-15, 0-20, 0-25 fm/c, total) into the total thermal photon yield, evaluated at $dN/dy = 12000$ (left) and $dN/dy = 6000$ (right).

Similar to 1+1 dimensional case we investigate dependence on the parameters of the model. In particular on initial, transition and freeze-out temperatures. Yields of thermal and decay photons, evaluated with three different initial temperatures ($T_{in} = 1 \text{ GeV}$, 500 MeV and 300 MeV), and fixed multiplicity, transition and freeze-out temperatures (17) are shown on the fig. 9, left plot. If one compare spectrum of thermal photons, evaluated within 1+1 (fig. 4, right plot) and 2+1 (fig. 9) Bjorken hydrodynamics, one finds, that in the case of $T_{in} = 1 \text{ GeV}$ hard parts of spectra of thermal photons coincide. So one can conclude, that both in 1+2 and 1+1 cases the system on initial stages cools predominantly due to longitudinal expansion. For lower initial temperatures $T_{in} = 500 \text{ MeV}$ and especially $T_{in} = 300 \text{ MeV}$ thermal photon spectra evaluated within 2+1 hydrodynamics are harder. This is evidence, that emission from later stages with lower temperature, but higher radial velocity and thus high effective temperature (20) dominate over emission from QGP.

Sensitivity of the yields to the variations of transition and freeze-out temperatures are shown on the fig. 9, right plot. Evaluations with basic set of parameters (17) (solid lines), higher transition temperature $T_c = 200 \text{ MeV}$ (dotted lines), and lower freeze-out temperature $T_f = 120 \text{ MeV}$ (dashed lines) are shown. In all three cases decay photons goes very close to each other. The same are thermal photons, however decreasing of T_f slightly increase yield of intermediate thermal photons.

In all previous calculations we used the simplest equation of state (EoS) – EoS with first order phase transition with ideal gas of quarks and gluons (degeneracy $g_{QGP} = 37$) in one phase and ideal gas of massless pions (degeneracy $g_{hadr} = 3$) in the other phase. Such EoS includes large jump in of specific entropy, and thus result in long living mixed phase. Besides this, such EoS leads to maximal possible velocity of sound $v_c = \sqrt{1/3}$ both in QGP phase and hadronic phase and thus maximal possible radial velocity at fixed value and spatial distribution of initial energy. If one considers massive hadrons instead of massless, and interacting quarks and gluons instead of free ones, then one finds $v_c < \sqrt{1/3}$. In addition, this inclusion of heavier hadrons and resonances in hadronic gas significantly increase its degeneracy and reduce jump of entropy. These effects result in decreasing of the yield of thermal photons in intermediate region.

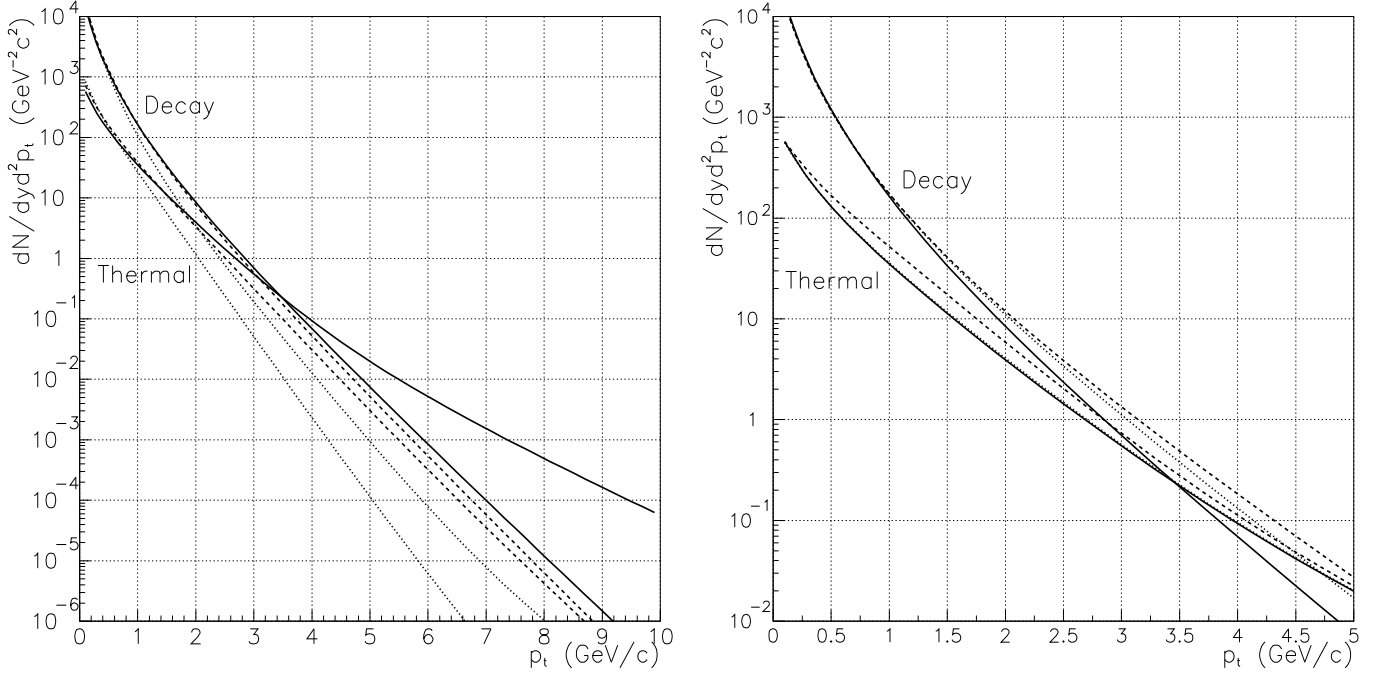


FIG. 9. Left plot: yield of thermal and decay photons, evaluated within 2+1 hydrodynamics with set the of parameters (17) and initial temperature $T_{in} = 1 GeV$ (solid lines), $T_{in} = 500 MeV$ (dotted lines) and $T_{in} = 300 MeV$ (dashed lines). Right plot: predictions with the basic set of parameters (17) (solid lines), variation of transition temperature $T_c = 200 MeV$ (dotted lines) and freeze-out temperature $T_f = 120 MeV$ (dashed lines). In all evaluations emission rates (5) (6) and (9) are used.

Another phenomenon perhaps important in evaluation of direct photon emission in ultrarelativistic heavy ion collision is absence of chemical equilibrium in the QGP phase. It was argued [15,23–25] that in the very beginning of collision quarks and gluons are strongly undersaturated (approximately 0.1 of equilibrium multiplicity), and subsequently their number is increased due to reactions $gg \leftrightarrow ggg$, $gg \leftrightarrow q\bar{q}$ etc. Because of comparatively small coupling constant, chemical equilibration is reached rather slowly – see fig. 10, left plot, with results from ref. [25]. In these evaluations initial conditions are taken from HIJING event generator, and then Boltzmann equation was solved with collisional term including all possible QCD binary interactions as well as reaction $gg \leftrightarrow ggg$, included to describe establishing of chemical equilibrium. Solid lines on the fig. 10 correspond to the evaluations with fixed $\alpha_s = 0.3$, and dashed lines – to evaluations with running coupling constant

$$\alpha_s(\langle E \rangle) = \frac{4\pi}{9 \ln(\langle E \rangle^2 / \Lambda_{QCD}^2)},$$

where $\langle E \rangle$ – average energy of partons evolved. As one can see from this figure, due to higher coupling, gluons come to the equilibrium faster than quarks and rate of equilibration practically independent on α_s . In contrast to them quarks equilibrate much slower, and this process strongly depends on α_s . However, one should take these evaluations with care: cross sections, entering collisional term has Coulomb divergency. To screen them one has to introduce cuts on soft quark and gluon exchange from some considerations, and result should be very sensitive to the chosen values of these cuts.

Yield of thermal photons emitted from QGP, evaluated within this approach with accounting of Compton scattering and annihilation and with time dependent α_s , is shown on fig. 10, right plot, by solid line. We compare this yield with one, evaluated within 2+1 Bjorken hydrodynamics with different initial temperatures and using emission rate (4) i.e. also including only Compton scattering and annihilation. We find that in the case of absence of chemical equilibrium yield of thermal photons decrease by $10^{-3} - 10^{-1}$.

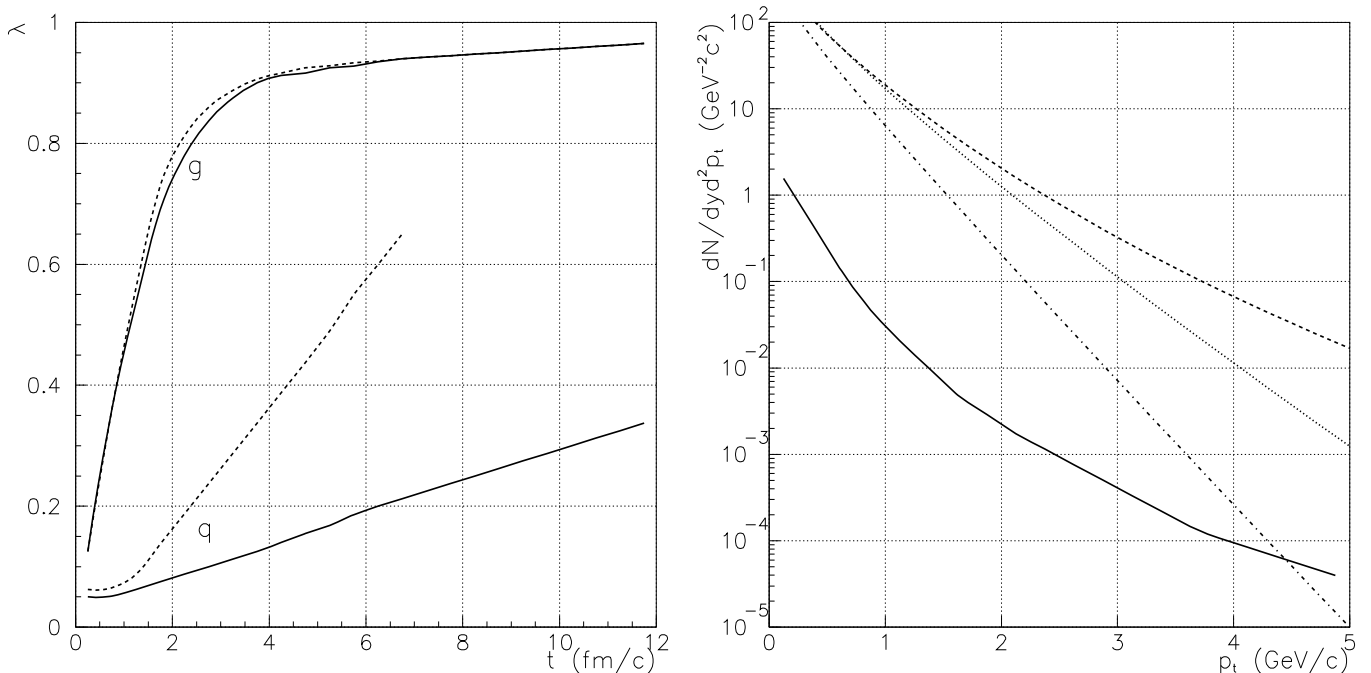


FIG. 10. Left plot: fugacity of quarks and gluons at LHC, solid lines – fixed α_s , dotted lines – running α_s . Right plot: thermal photon yield from QGP without chemical equilibrium (solid line) and from 2+1 Bjorken hydrodynamics with $T_{in} = 1 \text{ GeV}$ (dashed line) $T_{in} = 500 \text{ MeV}$ (dotted line) and $T_{in} = 300 \text{ MeV}$ (dash-dotted line). Only Compton scattering and annihilation (emission rate (4)) are taken into account.

However absence of chemical equilibrium does not influence significantly on the yield of thermal photons. As we have seen on fig. 8, due to significant radial velocity contribution of the hadronic gas, it is approximately the same as contribution of the hot phase. So even disappearing of the emission from the hottest stage does not reduce total yield of thermal photons more than several times.

D. Thermal photons from QGP and hadronic gas

From the point of view of registration of QGP it is important to know, whether or not thermal photons from QGP dominate over the thermal photons from hadronic gas. From one hand, thermal photons emitted from QGP have highest temperature, from the other hand thermal photons from hadronic gas have higher radial collective velocity, so that the answer is not obvious. In the paper [7] it was shown, that within 2+1 Bjorken hydrodynamics and emission rate (4) the contribution from QGP is slightly smaller than contribution from hadronic gas. However, in the recent paper [26], emission of thermal photons was evaluated with a rate accounting bremsstrahlung (5) and annihilation with scattering on third particle (6). It was shown, that in this case even for initial temperatures $T_{in} \sim 500 \text{ MeV}$ emission from QGP dominate over emission from hadronic gas. It is interesting, that in this case energy carried out by thermal photons becomes comparable with energy carried by final hadrons, and evolution of the system should be corrected to take into account energy loss due to thermal photon emission.

One can estimate yield of thermal photons from QGP and hadronic gas from fig. 8. Third curve from the bottom corresponds to the time ($\tau < 10 \text{ fm}$) of life of QGP phase. This curve should be compared with total photon yield. In the case of initial temperature $T_{in} = 1 \text{ GeV}$ and $dN/dy = 12000$ (left plot) contribution of QGP is approximately twice smaller than total photon yield, what means, that contributions of QGP and hadronic gas are comparable even at $p_t \sim 5 \text{ GeV}/c$. In the case $dN/dy = 6000$ (right plot) relative contribution of hadronic gas is smaller and QGP photons could dominate.

E. Direct photons at SpS

Below we compare spectra of thermal photons in Pb+Pb collisions at $158 A \cdot GeV$ (SpS), predicted by various models, with preliminary experimental results, obtained by WA98 collaboration. Our goal is not to choose model, which better describes experimental results or even to conclude, whether or not QGP was formed in these collisions. We just would like to demonstrate, that calculations within 2+1 Bjorken hydrodynamics can reproduce measured spectrum of thermal photons, providing we guessed appropriate initial conditions. As well we show, that at least at this energy different models give very similar predictions, so it is possible, that at LHC energy these predictions will be close too.

Let us begin from 2+1 Bjorken hydrodynamics. In this case we fix $T_c = 160 MeV$, $T_f = 140 MeV$ and choose initial conditions $T_{in} = 320 MeV$, $\tau_{in} = 0.4 fm/c$ so that reproduce multiplicity $dN/dy = 620$ and spectrum [27] of final photons. Quality of the data description can be seen on the fig. 11, left plot. Having parameters of the model fixed, we evaluated yield of thermal photons using two emission rates of thermal photons: in the first case we use emission rate (4) both in QGP and hadronic gas phase and in the second case - emission rate (5), (6) for QGP phase and (9) for hadronic gas phase. Evaluated yields of thermal photons are shown on the fig. 11, right plot, by thin dashed line and thin solid line for the two cases respectively. Experimental data are shown by rectangles.

Second hydrodynamic model we consider is fully hydrodynamic (3+1 dimensional) model [9]. Yield of thermal photons, evaluated within this model is shown by thick solid line. In these evaluations emission rate (4) for QGP and (9) for hadronic gas was used. However, the difference between predictions of these models arises not from type of longitudinal expansion - scaling or hydrodynamic, but from initial conditions: in the 3+1 hydrodynamics they are evaluated in spirit of Landau hydrodynamics (shock waves propagate through the colliding nuclei and heat up the system). Such description of initial stage of collision results in higher initial temperatures compared to usually considered in Bjorken scenarios, so one finds higher effective temperatures of thermal photons.

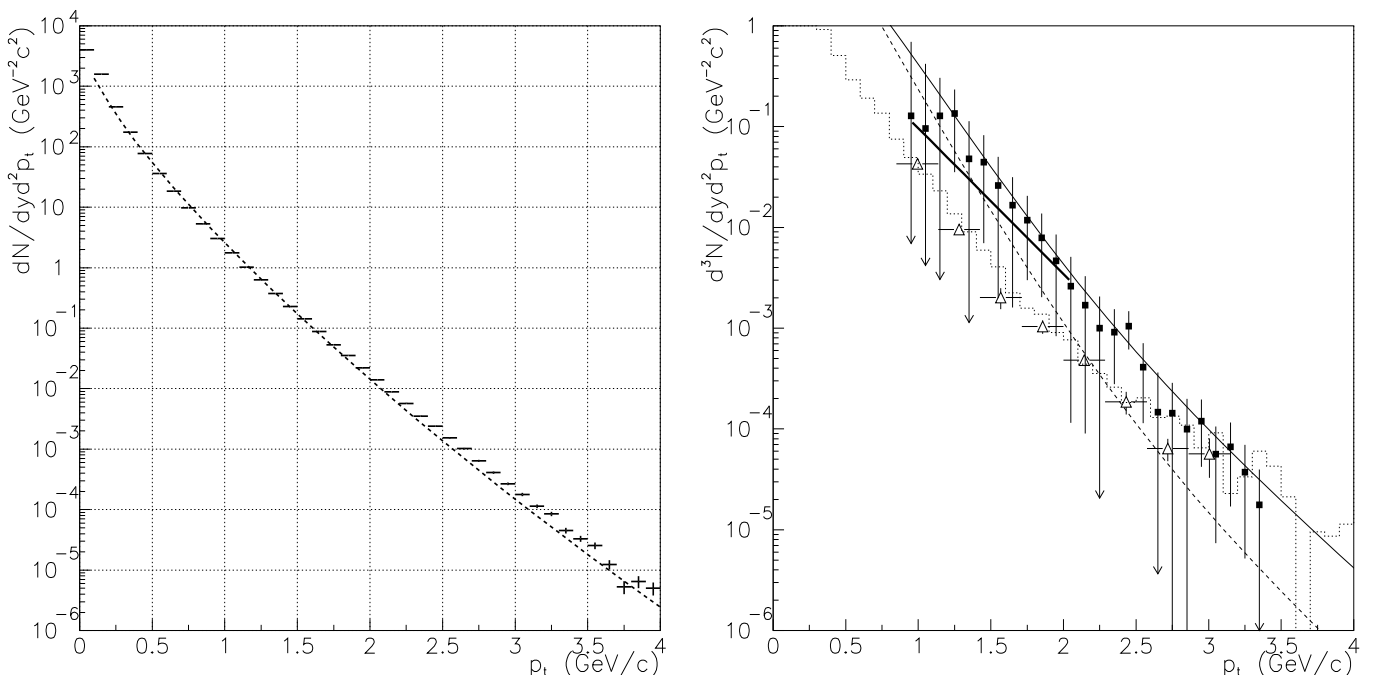


FIG. 11. Left plot: total photon yield in Pb+Pb collision at $158 A \cdot GeV$, measured by WA98 collaboration, preliminary data, (crosses) and evaluated within 2+1 Bjorken hydrodynamics (dashed line). Right plot - yield of direct photons in this collision. Rectangles - preliminary WA98 results, dashed histogram - predictions of Parton Cascade Model, triangles - predictions of UrQMD, thick solid line - 3+1 hydrodynamics, thin solid and dashed lines - 2+1 Bjorken hydrodynamics with emission rate accounting of bremsstrahlung and contribution of a_1 resonance and without accounting of these effects correspondingly.

To compare predictions of equilibrium (hydrodynamic) models with nonequilibrium (cascade) models we consider as well predictions of Partonic Cascade Model (PCM) [28] and Ultrarelativistic Quantum Molecular Dynamic Model (UrQMD) model [29]. PCM describes nucleus-nucleus collisions in terms of parton picture of hadronic interactions. It

performs evolution using quantum kinetics with interactions of quarks and gluons, evaluated within pQCD. Developed partonic picture clusterizes to form final hadrons. Predictions of this model for $Pb + Pb$ collisions at $160 A \cdot GeV$, taken from [28], are shown on fig. 11, right plot, by dotted histogram. In contrast to PCM, the second cascade model, UrQMD, deals with propagation and interactions of hadrons in hot matter. Yield of direct photons in $Pb + Pb$ collisions at $160 A \cdot GeV$ evaluated within this model, taken from [29], is shown on fig. 11, right plot, by triangles.

Comparing predictions of all considered models one finds that they go rather close to each other. Moreover, comparing PCM and UrQMD one finds a striking coincidence of their predictions. It looks like the yield of direct photons is independent on the details of the interactions of particles in the hot matter. As for 2+1 Bjorken hydrodynamics, one can see, that yield, evaluated with accounting of bremsstrahlung and annihilation with rescattering on third particle gives the best description of experimental data among considered models. So we conclude, that 2+1 Bjorken model provides reasonable description of evolution of hot matter, such as we obtain good reproduction of the yield of thermal photons.

Another important observation, we can made from fig. 11, is that in the range $p_t < 5 GeV/c$ predictions of all considered models differ less than order of magnitude.

III. DECAY PHOTONS

In the previous sections we evaluated yield of thermal photons. However from the experimental point of view not only its absolute value but also ratio of spectra of thermal and total photons is important. It is this ratio, which controls possibility of extraction of thermal photons from the total photon yield. To estimate total photon yield we have to evaluate spectrum of decay photons, i.e. to evaluate p_t distributions of π^0 , η , etc. hadrons, having channels of decay onto photons, and decay them into photons. To do this we use several models: 2+1 Bjorken hydrodynamic model, HIJING 1.36 and VENUS 4.12 event generators.

On the fig. 12 we present results of hydrodynamic calculations of yields of decay photons for three values of initial temperature $T_{in} = 1 GeV$, $T_{in} = 500 MeV$ and $T_{in} = 300 MeV$, and compare them with predictions of HIJING 1.36 and VENUS 4.12 models.

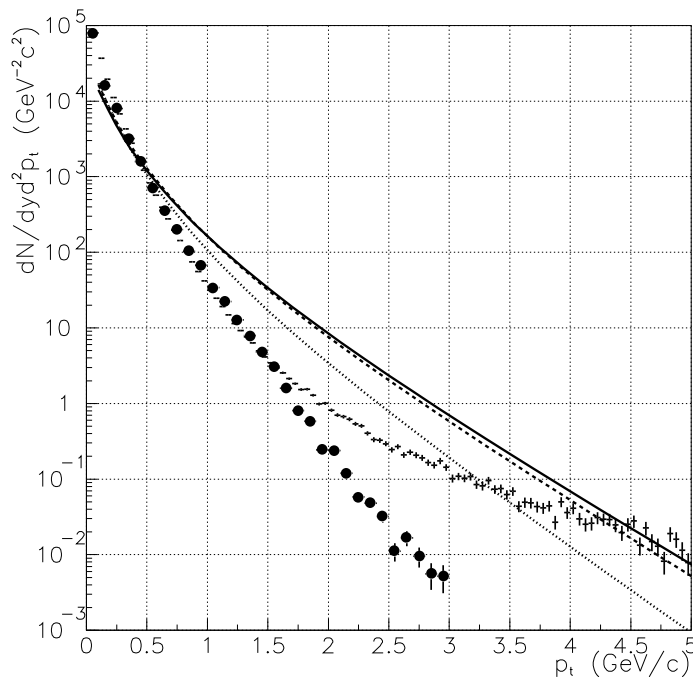


FIG. 12. Total photon yield in $Pb + Pb$ collision at LHC energy, evaluated within 2+1 Bjorken hydrodynamics with initial temperatures $T_{in} = 1 GeV$ (solid line), $T_{in} = 500 MeV$ (dashed line) and $T_{in} = 300 MeV$ (dotted line). Crosses – predictions of HIJING 1.36, circles – predictions of VENUS 4.12.

HIJING is model of heavy ion collisions, which consider initial stage of collision (jet and minijet production) on the basis of perturbative QCD, and describe fragmentation of created partons using Lund string model [32]. HIJING does not include interactions of the secondary particles. This results in nonexponential p_t distribution with excess of high

energy and lack of intermediate energy particles in comparison with thermal distribution. In contrast to HIJING, VENUS takes into account rescattering of final particles [33] and thus results in exponential spectrum, closer to the predictions of hydrodynamic model. However, VENUS does not include radial flow, so that spectrum predicted by this model is softer than one, predicted by hydrodynamics. In evaluations of the ratio thermal to decay photons we use predictions of spectrum of decay photons from hydrodynamic model and HIJING.

If one uses p_t distribution of decay photons, given by HIJING 1.36, (see fig. 13, left plot) then one finds, that thermal photons dominate over decay photons in the intermediate region for all considered initial temperatures. This takes place because of rather special shape of p_t distribution of final hadrons, predicted by HIJING. In contrast to this, if one evaluates both thermal and decay photons within hydrodynamic model (see fig. 13, right plot), then for initial temperatures $\sim 300 MeV$ there will be region, where ratio reached its maximal value and position of the maximum is shifted to hard part with increasing of initial temperature, while at $T_{in} \sim 500 MeV$ becomes approximately constant. For higher initial temperatures contribution of thermal photons increase with increasing of p_t .

If one consider only leading order α_s reactions in QGP – Compton scattering and annihilation, then the ratio Thermal/Total reaches 20% in maximum even for lower considered initial temperature. If one includes higher order α_s corrections – bremsstrahlung and annihilation with rescattering on third particle, then the ratio Thermal/Total, evaluated for $T_{in} = 300 MeV$ reaches 30-40%.

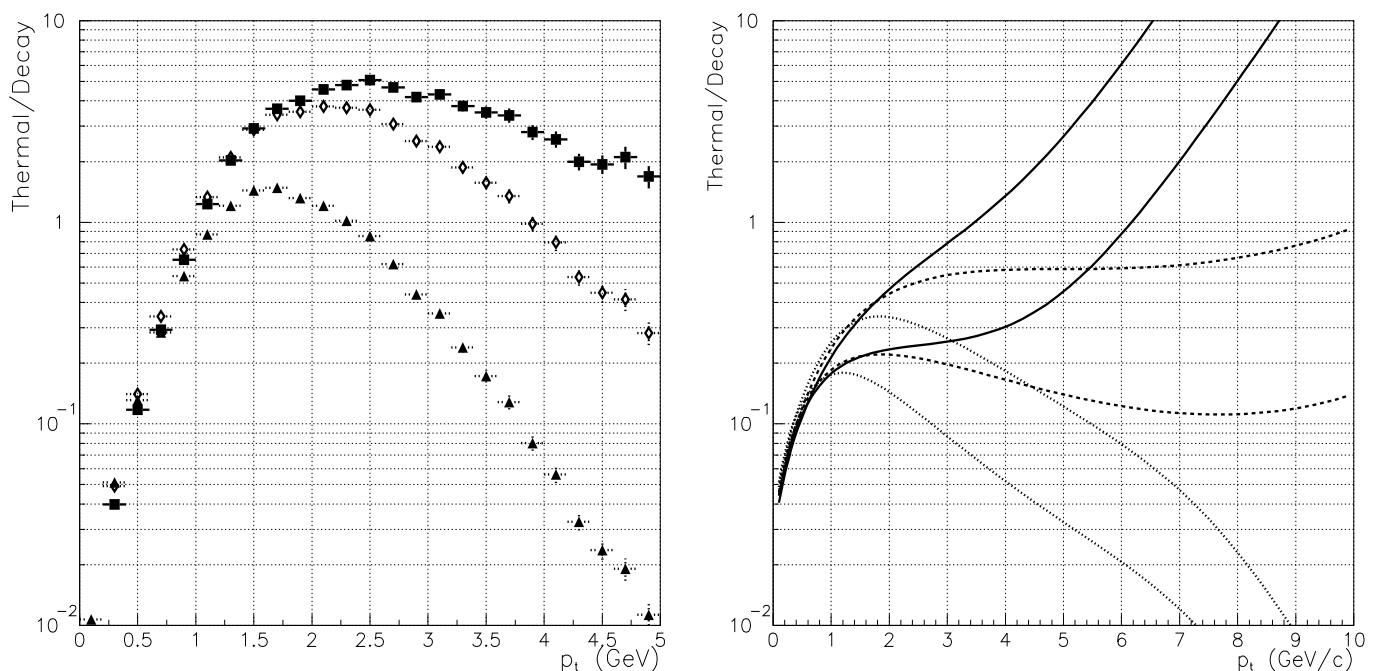


FIG. 13. Ratio yield of thermal to yield of decay photons in $Pb + Pb$ collision at LHC energy. Left plot: Thermal photons, evaluated within 2+1 Bjorken hydrodynamics, are divided by decay photons, taken from HIJING. Rectangles correspond to thermal photons, evaluated with initial temperatures $T_{in} = 1 GeV$, diamonds – $T_{in} = 500 MeV$ and triangles – $T_{in} = 300 MeV$, in all cases emission rate (4) was used. Right plot: both thermal and decay photons are evaluated within 2+1 Bjorken hydrodynamics. Solid lines correspond to initial temperature $T_{in} = 1 GeV$, dashed – $T_{in} = 500 MeV$ and dotted – $T_{in} = 300 MeV$, lower lines evaluated with emission rate (4), upper – with emission rates (5), (6) and (9).

IV. CONCLUSION

We have considered emission of prompt, thermal and decay photons in $Pb + Pb$ collisions at SpS and LHC energies and estimated uncertainty in predictions of their yields. We find, that main uncertainty in the yield of prompt photons comes from the lack of precise knowledge of structure functions at small x and their modifications in nuclei. This leads to variations of the yield of prompt photons within factor ~ 3 .

For thermal photons situation is more complicated. The main source of uncertainty comes from impossibility to describe uniquely evolution of heavy ion collisions. For description of evolution the both kinetic and hydrodynamic models are used. We compared predictions of kinetic and hydrodynamic models at SpS energy, however for LHC

energy we concentrated on hydrodynamic models. We find, that hard part of the spectrum $p_t > 4 - 5 \text{ GeV}$ slightly depends on the presence of the radial flow (compare figs. 4 for 1+1 expansion and 9 for 2+1). This takes place because this region of p_t is populated due to emission from the initial stage (see fig. reftimes) when radial flow is not developed yet. Even if extremely high initial temperatures are created in the beginning of the collision, they are slightly affect on the radial flow, because as a result of longitudinal expansion the high temperatures lives very short time and can not accelerate considerably the matter in radial direction. This is illustrated on the fig. 9: difference of the effective temperatures of decay photons, evaluated at $T_{in} = 1 \text{ GeV}$ and $T_{in} = 500 \text{ MeV}$ is smaller, than difference between $T_{in} = 500 \text{ MeV}$ and $T_{in} = 300 \text{ MeV}$. So, we find that for hard part of spectrum 1+1 and 2+1 hydrodynamics models give similar predictions. However, 2+1 Bjorken hydrodynamics is not quite two-dimensional – longitudinal expansion in it is scaling. Comparing predictions of 1+1 Bjorken and 1+1 Landau hydrodynamics we show, that this is not important for the case of thermal photons.

In addition to ambiguity in description of evolution, there is significant uncertainty in the emission rate: inclusion of the higher order α_s corrections result in increasing of it up to order of magnitude.

We show, that hard part of thermal photon distribution is sensitive to the scenario of collision. If fast thermalization of colliding nuclei with high initial temperature takes place, than one finds high yield of thermal photons, otherwise, if string-tube model of thermalization takes place, then yield of thermal photons in hard part will be much smaller.

We estimated the ratio of Direct/Decay photons at LHC energy and find it large enough (20 – 30%) to be measured by ALICE PHOS setup, whose expected sensitivity to the direct photons is approximately 5% [34]. So that thermal photons considerably contribute into total photon yield. If thermal photons from QGP are evaluated without accounting of bremsstrahlung and annihilation with scattering on third particle, then yield of thermal photons from hadronic gas exceeds yield of thermal photons from QGP [7]. Otherwise, if one takes into account these higher order α_s corrections, then thermal photons from QGP dominates over photons from hadronic gas [26].

The authors would like to thank V.I. Manko for interest and useful discussions. This work was supported by grant RFFI 96-15-96548.

- [1] D. Yu. Peressounko, Yu. E. Pokrovsky, Nucl.Phys. **A624** (1997) 738.
- [2] E. V. Shuryak, Phys. Lett. **B78** (1978) 15.
- [3] R.C. Hwa and K. Kajantie, Phys. Rev. **D32** (1985) 1109.
- [4] M. Neubert, Z. Phys. **C42** (1989) 231.
- [5] R. Baier et al., Z. Phys. **C53** (1992) 433.
- [6] P.V. Ruuskanen, Nucl. Phys. **A544** (1992) 169c.
- [7] J. Alam, D.K. Srivastava, B. Sinha, D.N. Basu, Phys. Rev. **D48** (1993) 1117.
- [8] J. Kapusta, Nucl. Phys. **A566** (1994) 45c.
- [9] N. Arbx, U. Ornik, M. Plumer, A.Timmermann, R.M. Weiner, Phys. Lett. **B 345** (1995) 307.
- [10] John J. Neumann, David Seibert, George Fai, Phys.Rev. **C51** (1995) 1460.
- [11] C. M. Hung, E. V. Shuryak, Phys.Rev. **C56** (1997) 453.
- [12] N. Hammon, A. Dumitru, H. Stoecker, W. Greiner, Phys. Rev. **C57** (1998) 3292.
- [13] J. Kapusta, P. Lichard and D. Seibert, Phys. Rev. **D44** (1991) 2774.
- [14] P. Aurenche, F.Gelis, R. Kobes, H. Zaraket, Phys.Rev. **D58** (1998) 085003, hep-ph/9804224.
- [15] C.T. Traxler and M.H. Thoma, Phys. Rev. **C 53** (1996) 1348.
- [16] R. Baier, M. Dirks, K. Redlich, D. Schiff, Phys. Rev. **D 56** (1997) 2548.
- [17] A.Dumitru, D.H. Rischke, H. Stoecker, W. Greiner, Mod. Phys. Lett. **A 8** (1993) 1291.
- [18] L. Xiong, E. Shuryak, G.E. Brown, Phys. Rev. **D46** (1992) 3798.
- [19] S. Sarkar, J. Alam, P. Roy, A.K. Dutt-Mazumder, B. Dutta-Roy, B. Sinha, Nucl. Phys. **A634** (1998) 206.
- [20] J. D. Bjorken, Phys. Rev. **D 27** (1983) 140.
- [21] J. Cleymans, K. Redlich, D.K. Srivastava, Phys. Lett. **B 420** (1998) 261.
- [22] Yu.A. Tarasov, V.G. Antonenko, Z.Phys., **C 66** (1996) 215.
- [23] E.Shuryak and L. Xiong, Phys. Rev. Lett. **70** (1993) 2241.
- [24] M. Strickland, Phys. Lett. **B 331** (1994) 245.
- [25] S.M.H. Wong, Phys. Rev. **C58** (1998) 2358; nucl-th/9810081.
- [26] D.K. Srivastava, e-print nucl-th/9904010
- [27] T. Peitzmann et al., Nucl. Phys. **A610** (1996) 200c.
- [28] D.K. Srivastava, K. Gaiger, Phys. Rev. **C 58** (1998) 1734.

- [29] A. Dumitru, M. Bleicher, S.A. Bass, C. Spieles, L. Neise, H. Stocker, W. Greiner, Phys. Rev. **C57** (1998) 3271.
- [30] D.W. Duke, J.F. Owens, Phys. Rev. **D22** (1984) 2280.
- [31] M. Gluck, E. Reya, A. Vogt, Z. Phys. **C67**, (1995) 433.
- [32] Xin-Nian Wang and M. Gyulassy, LBL-31036.
- [33] K. Werner, Phys. Rep. **232** (1993) 87.
- [34] ALICE Technical Proposal, CERN/LHCC/95-71.